Medical Image Analysis 60 (2020) 101588

Contents lists available at ScienceDirect

Medical Image Analysis

journal homepage: www.elsevier.com/locate/media

A partial augmented reality system with live ultrasound and registered preoperative MRI for guiding robot-assisted radical prostatectomy

Golnoosh Samei[a,*], Keith Tsang[a], Claudia Kesch[b], Julio Lobo[a], Soheil Hor[c], Omid Mohareri[d], Silvia Chang[e,f], S. Larry Goldenberg[b], Peter C. Black[b], Septimiu Salcudean[a,*]

[a] Department of Electrical and Computer Engineering, University of British Columbia, Vancouver, BC V6T 1Z4, Canada
[b] Vancouver Prostate Centre, Department of Urologic Sciences, University of British Columbia, Vancouver, BC V5Z 1M9, Canada
[c] Department of Electrical Engineering, Stanford University, Stanford, CA 94305, USA
[d] Surgical Intuitive, Sunnyvale, CA 94086, USA
[e] Department of Radiology, University of British Columbia, Vancouver Hospital and Health Sciences Center, Vancouver, British Columbia, Canada
[f] Department of Pathology and Laboratory Medicine, University of British Columbia, Vancouver, Canada

ARTICLE INFO

Article history:
Received 24 January 2019
Revised 31 July 2019
Accepted 10 October 2019
Available online 29 October 2019

JEL classification:
41A05
41A10
65D05
65D17

Keywords:
Image-guidance
Surgery
Ultrasound
Magnetic resonance imaging
Image fusion
Registration

ABSTRACT

We propose an image guidance system for robot assisted laparoscopic radical prostatectomy (RALRP). A virtual 3D reconstruction of the surgery scene is displayed underneath the endoscope's feed on the surgeon's console. This scene consists of an annotated preoperative Magnetic Resonance Image (MRI) registered to intraoperative 3D Trans-rectal Ultrasound (TRUS) as well as real-time sagittal 2D TRUS images of the prostate, 3D models of the prostate, the surgical instrument and the TRUS transducer. We display these components with accurate real-time coordinates with respect to the robot system. Since the scene is rendered from the viewpoint of the endoscope, given correct parameters of the camera, an augmented scene can be overlaid on the video output. The surgeon can rotate the ultrasound transducer and determine the position of the projected axial plane in the MRI using one of the registered da Vinci instruments. This system was tested in the laboratory on custom-made agar prostate phantoms. We achieved an average total registration accuracy of 3.2 ± 1.3 mm. We also report on the successful application of this system in the operating room in 12 patients. The average registration error between the TRUS and the da Vinci system for the last 8 patients was 1.4 ± 0.3 mm and average target registration error of 2.1 ± 0.8 mm, resulting in an *in vivo* overall robot system to MRI mean registration error of 3.5 mm or less, which is consistent with our laboratory studies.

1. Introduction

Radical prostatectomy (RP), the surgical removal of the prostate gland, is a standard treatment of organ-confined prostate cancer. The primary goal of the surgery is to remove the entire prostate and in particular all cancerous tissues (oncological success), while sparing the critical structures adjacent to the cancer (functional success), hence preserving continence and potency. The difficulty of RP lies in the delicate trade-off between these two conflicting goals; ensuring oncological success could compromise the ability to achieve functional success. Currently, the rates of positive surgical margins (PSM), i.e., presence of cancer cells at the edge of the excised tissue, are reported to be ranging from 9.6% to 26% for robot-assisted RP (Ficarra et al., 2009; Haglind et al., 2015). Side effects of erectile dysfunction and urinary incontinence affect up to 70% and 21% of patients, respectively (Haglind et al., 2015).

Robot-assisted laparoscopic radical prostatectomy (RALRP) provides an ideal platform for integrating image guidance into the surgical environment and, therefore, has the potential to improve functional and oncological outcomes. Trans-rectal ultrasound (TRUS) is the medical imaging modality of choice to guide prostate interventions, as it is real-time, accessible, and can be easily integrated in the RP procedure. Its application in image guidance systems during RALRP has been shown to decrease the rate of PSM and improve the dissection of the neurovascular bundles (Ukimura et al., 2006). Robotic TRUS has been used in RALRP with reported success by a number of groups (Han et al., 2011; Hung et al., 2012; Long et al., 2012). Hung et al. (2012) reported difficulties in using a foot pedal to control the TRUS. To allevi-

* Corresponding author.
E-mail addresses: sameig@ece.ubc.ca (G. Samei), tims@ece.ubc.ca (S. Salcudean).
URL: http://www.ece.ubc.ca/~tims (S. Salcudean)

https://doi.org/10.1016/j.media.2019.101588
1361-8415/

ate the overhead of manually controlling the TRUS probe during surgery, Mohareri et al. (2015a) proposed a robotic TRUS system that is registered to the da Vinci system by using a simple and accurate procedure, enabling the TRUS sagittal imaging plane to be controlled by one of the da Vinci instruments, directly from the robot console.

While B-mode ultrasound is sufficient for imaging the prostate, it cannot be used to accurately image isoechoic lesions and identify prostate cancer (PCa). T_2 weighted (T2) magnetic resonance imaging (MRI) produces detailed anatomical images of the prostate and its internal structure, the seminal vesicles, and the external urethral sphincter (Villeirs and De Meerleer, 2007). Multiparametric MRI (mp-MRI) is the most accurate method for imaging PCa. To leverage its accuracy, needle-based systems for biopsy and brachytherapy within the bore of the MRI scanner have been developed (Susil et al., 2004; Cepek et al., 2013). However, surgery within the bore of the MRI is not possible with current technology. The application of mp-MRI for surgery planning has been reported by groups such as (Tan et al., 2012). They suggest that MRI could be used to evaluate whether the spread of disease includes the seminal vesicles and the neurovascular bundles (NVB), and whether the surgical approach spares a sufficient length of the urethra to allow a fast return to continence. They showed that 93% of high-risk patients and 67% of low-risk patients who had preoperative MRI had appropriate NVB resection/preservation due to MRI findings. MRI has also been used to change initial surgical plans in 28% of patients (McClure et al., 2012); 61% of changes were to nerve sparing; 39% were changed to non-nerve sparing. In every case in which the surgery was changed to nerve sparing, surgical margins were negative on the side of the change. RP planning based on MRI demonstrates the potential of MRI-guided RP. However, the MR images are not updated or deformed based on the current positioning of the patient; hence cancer localization is only approximate and relies on the cognitive transformation by the surgeon from MRI coordinates to the patient. Martini et al. (2019) conclude in their review of image guided systems for robot assisted surgeries that despite its benefits, mp-MRI is still underused in planning for robotic prostatectomy.

In a robot-assisted surgery setting, augmented reality (AR) has the potential to provide much-needed visualization. Simpfendörfer et al. (2011) presented an AR navigation system for TRUS-guided conventional laparoscopic RP. To compute the registration between the laparoscopic video and the TRUS model, navigation aids in the form of needles with colored heads were inserted into the prostate. These needles were manually segmented in a reference 3D TRUS and continuously and automatically tracked in the laparoscopic video images. Their system was used in one human in-vivo case without complications. Bernhardt et al. (2017) provide a review on the status of AR in laparoscopic surgery as of 2016. More recently, Kolagunda et al. (2018) presented a mixed reality guidance system for RALRP that was connected to a head-mounted visualization device. They used the stereoscopic images from the laparoscope in the da Vinci robot to obtain a 3D reconstruction of the surface of the prostate. The resulting point cloud was registered to the 3D model of the prostate obtained from a preoperative MRI. Their method was not real-time; it took approximately 3 min to render the 3D prostate model and overlay it on a recorded pair of stereoscopic images. Moreover, they needed to calibrate the stereo laparascopic cameras before the surgery to be able to obtain a correct 3D surface reconstruction. However, this would require that the surgeon refrains from changing the focus of the camera during the entire surgery which limits the applicability of their method. Kratiras et al. (2018) report on a phase I study where they tested a tablet-based guidance software for RALRP. Their system utilizes the preoperative MRI of the prostate, and maps the images intraoperatively in real-time to the patient by magnetic tracking to fixed points of the patient's pelvis. As noted in (Kolagunda et al., 2018), the use of a different display from the surgeon's console precludes the system being used by the operating surgeon in current clinical robot-assisted systems. Perhaps the most advanced AR system for RALRP is that of Porpiglia et. al presented in a number of recent publications (Porpiglia et al., 2018a,b,c,d). Their AR-RALRP system is based on mp-MRI and has been employed in a phase II study on 30 patients. The 3D prostate model was constructed from contouring on mp-MRI and was overlaid on the laparoscopic video feed rigidly using a manual process. The output was displayed on the da Vinci system's surgeon console using the TilePro™ functionality. To ensure correct alignment of the model on the organ, a professional had to manually track and readjust the 3D model during the surgery through graphics software. To evaluate the system, the positions of the lesions as indicated by the virtual model were marked by metallic clips during the surgery and examined *ex vivo* and reported to be correct. In addition to this evaluation scheme, they compared the surfaces of the 3D reconstructed virtual model and the scanned *ex vivo* prostate and reported the mismatch to be between 1 to 5 mm. While this shows a small deviation between the shape of the prostate at the time of MRI acquisition and after excision, it does not provide an error of the registration during the surgery or in the presence of organ deformation or enlargement.

Although reports indicate that surgeons are interested in the technology (Ukimura et al., 2014; Thompson et al., 2013; Cohen et al., 2010), there are limited reports of fused MRI-TRUS guidance for RP as outlined in a review paper by Sridhar et al. (2013). Ukimura and Gill (2008) proposed a system for use with conventional laparoscopic prostatectomy in which the preoperative MRI is fused with a 3D image reconstructed from the intraoperative TRUS scan. More recently they developed a surgical navigation model and tested it in RALRP of 10 patients (Ukimura et al., 2014). A 3D model was created based on 3D TRUS-guided prostate biopsies. Five key anatomic structures (prostate, biopsy-proven cancer lesion, neurovascular bundles, urethra, and recorded biopsy trajectories) were marked on the 3D prostate model which was displayed next to the endoscope's feed. They achieved negative surgical margins in 90% of patients and at postoperative 3 months, prostate-specific antigen levels were undetectable (< 0.03 ng/mL). The placement and orientation of the 3D model was done manually by a urologist.

While the use of MRI-TRUS-guidance is limited in RP, there are several such systems for biopsy, as surveyed by Logan et al. (2013). These include commercialized systems such as the Biopsee (MedCom, Darmstadt, Germany), UroNav (Invivo Corporation, Gainesville, Florida), Artemis (Eigen, Grass Valley, USA) and Urostation® (Koelis, France). In general, it has been shown that MRI-TRUS fusion yields a higher tumour-positive percentage per biopsy (Pinto et al., 2011; Moore et al., 2013; Marks et al., 2013). The systems described above require manual positioning and control of the TRUS transducer and are not usable for RALRP where the surgeon is sitting at the console and not at patient's side. Nevertheless, they demonstrate the usefulness of the MRI-TRUS fusion approach.

We propose a virtual reality-based image guidance system for RALRP based on registering a preoperative MRI, annotated with regions of high cancer probability, to real-time, intraoperative TRUS images. By leveraging the intraoperative TRUS, the patient's registered preoperative MRI is displayed at the correct location with respect to the da Vinci instrument in the surgeon's console, with minimal interaction from the surgeon. Moreover, by non-rigidly registering the preoperative MRI to the TRUS, we are able to accurately compute the deformation of the tissue and update the 3D

Table 1
Connections between the system components and the data transferred between them. Connection number 6 is bidirectional.

#	Sender	Receiver	Connection type	Transferred data
1	PC	dV Console (TilePro™)	SDI	Guidance software output (L + R)
2	PC	Multimedia recorder	HDMI	PC Output (Video channel)+ API (Audio channel)
3	dV Vision cart	Multimedia recorder	SDI	Enodscope output (L + R)
4	US Machine	PC	HDMI-SDI	US
5	dV Vision cart	PC	Ethernet	API
6	Motor controller	PC	Serial-USB	Probe roll angle
6	PC	Motor controller	USB-Serial	Command signals

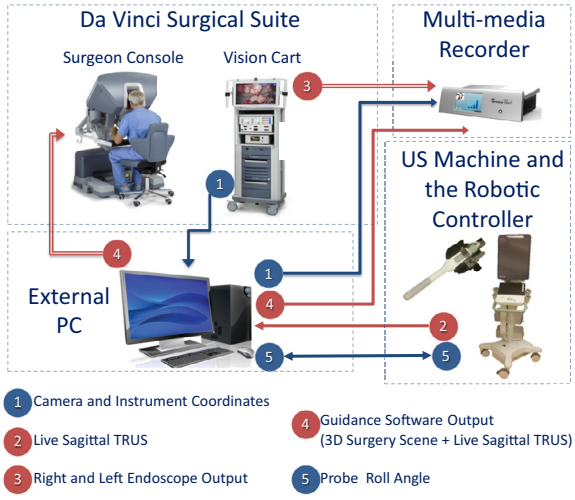

Fig. 1. Overview of the hardware setup of our image-guidance system.

model of the prostate during the surgery. The rendered scene in the console comprises:

- real-time sagittal/side-firing ultrasound from the TRUS probe, as described in Mohareri et al. (2015a), (Mohareri et al., 2015b), that tracks one of the da Vinci instruments in real-time;
- transverse preoperative MRI, deformably registered to the intra-operative 3D TRUS;
- 3D models of the prostate, the surgical instrument and the TRUS transducer.

These images are displayed in real-time, at the correct physical location with respect to the da Vinci coordinate system in which instruments are moving. Since the TRUS probe tracks the tip of a da Vinci surgical instrument and the TRUS volume is registered to the preoperative MRI volume, the surgical instrument is used as an intuitive and easy-to-use control device for the surgeon to view different slices of the prostate and surrounding tissue in both the MR and TRUS images. We also describe experiments to evaluate the overall accuracy of system and target registration errors in prostate phantoms.

2. Hardware setup

Fig. 1 gives an overview of our hardware setup as it was employed during the phantom experiments and the patient studies and Fig. 10 shows our hardware setup in the surgery room. It is comprised of (i) a *da Vinci*® surgical suite (Intuitive Surgical, Sunnyvale, California, United States) (ii) an ultrasound machine with a TRUS probe mounted on a 2 DOF robotic manipulator, (iii) A multimedia recorder to record the surgery for later analysis and (iv) an external computer for MR-TRUS registration, da Vinci-TRUS calibration, controlling the TRUS manipulator and rendering the 3D surgery scene.

The connections and the data transferred between the system components are described in detail in Table 1 and illustrated in Fig. 1. The data consist of sets of parameters (indicated with solid blue lines in Fig. 1) and images (indicated with double red lines in Fig. 1).

2.1. da Vinci system

We have access to two da Vinci systems. For the phantom studies in our research lab an S model was used while the surgeries in our collaborating hospital were performed using an Si model. During surgery, the Application Programming Interface (API) of the da Vinci system streams the 3D coordinates and orientation of the instruments and the endoscope to the external PC (DiMaio and Hasser, 2008).

2.2. Ultrasound machine and the robotic controller

A previously designed and clinically-used robotic controller is employed for automatic and remote rotation (angle range ±50 degrees) of the TRUS transducer during the procedure (Mohareri et al., 2015a).

A BK 3500 ultrasound machine (BK Medical, Herlev, Denmark) with an E14CL4b 14-4 MHz biplane transducer is used for imaging the prostate. It acquires ultrasound frames at a frequency of 34Hz. A standard brachytherapy stabilizer arm (Micro-Touch 610–911; CIVCO Medical Solutions, Kalona, IA, USA) is mounted on the operating table and the TRUS robot is installed on the stabilizer, as shown in Fig. 7a. The volumetric images are captured using the 192-element 65 mm long sagittal array with a transmission frequency of 9 MHz and an imaging depth of 65 mm, with the TRUS robot rotating the transducer about its long axis and collecting the 2D sagittal images at each angle increment. We use a 100-degree rotary sweep about the probe axis with images acquired at increments of 0.5 degrees. We interpolate these slices on a Cartesian grid to obtain a 3D TRUS image. The capture time is approximately 30s per volume. The roll angle set point and the actual roll angle of the probe are also transmitted between the external computer and the TRUS motor controller.

2.3. External computer

A standard Windows-based (Microsoft Redmond, WA, USA) desktop is used to run all the software required by the system. This computer has a BlackMagic Decklink Quad 2 frame grabber card (Blackmagic Design, Port Melbourne, Australia) which features eight independent input/output serial digital interface (SDI) ports. Two ports are used to stream the video produced by the guidance software to the da Vinci console left and right input channels using its TilePro™ in-console display system. One port is used to stream the live video from the ultrasound machine. All the video streams are produced at a resolution of 1920 × 1080 i at 59.94 Hz.

2.4. Multimedia recorder

An Ephiphan Pearl™ device is used to record the left and right channels of the da Vinci endoscope, the 3D surgery scene, the live TRUS B-Mode images and the raw API data. The endoscope's video stream is obtained from the SDI video output of the da Vinci vision cart. The reconstructed surgery scene is obtained from the desktop through a high-definition multimedia interface (HDMI) connection. The 3D surgery scene and TRUS images are cloned from the desktop display while the API data are encoded into an audio signal.

3. Image guidance software and methods

3.1. TRUS-da Vinci calibration

In order for the TRUS robot to automatically track the da Vinci instrument, a transformation from the TRUS coordinate system to the da Vinci coordinate system is obtained through a manual calibration process. We used the registration method introduced by Adebar et al. (2011) in which at least four points on the prostate surface are touched by a da Vinci surgical instrument and identified in the TRUS image. In our studies these points were two points at the apex and base on the midline, and two points on the midgland on the right and left (see Fig. 4). For each point, the probe's rotation angle is manually adjusted until the da Vinci instrument tip is visible in the image. The probe roll angle, the instrument's coordinates in the TRUS and the da Vinci coordinate systems are recorded. We used the RANSAC algorithm (Fischler and Bolles, 1981) to find the optimal transformation, $T_{\text{TRUS-DV}}$, between the selected pairs of points.

3.2. Preoperative MRI and intraoperative TRUS registration

The prostate position and shape during the surgery might differ from the preoperative MR, I_{MR}. This is because firstly, I_{MR} is usually acquired weeks before the surgery, and secondly, the patient's position during the MR acquisition is different from the RALRP surgery. Therefore, a deformable registration between I_{MR} and the intra-op TRUS has to be performed. We employed a linear stress-strain quasi-static finite-element model (FEM) for the deformation in our registration. An expert clinician contoured the prostate and the cancerous tissue on I_{MR} (Fig. 2b). Based on this contouring, we created a tetrahedral mesh and assigned appropriate tissue elasticity values to the elements within the prostate gland and its neighboring structures (Fig. 2c). The organ-specific tissue elasticity values could be either generic, such as those reported in the literature, or patient-specific by computing them from MRI elastography. In our experiments, we used a Young's modulus and Poisson's ratio pair of (50 kPa, 0.49) for the prostate and (15 kPa, 0.45) for the surrounding tissue based on previous research (Nir et al., 2013). Based on the FEM, the elastic response between the nodal displacements u and forces f of this discrete deformable tissue model (mesh) can be formulated as $f = Ku$, where K is the stiffness matrix. The nodes on the surface of the mesh bounding box are considered as the fixed boundary constraints and their corresponding rows and columns in the inverse stiffness matrix K^{-1} are set to zero. Generating the FEM model with the above steps can be performed prior to the surgery, once I_{MR} is available and the prostate and the cancerous tumours are delineated by the radiologist.

At the beginning of the surgery, a 3D TRUS volume, I_{US}, is acquired (Fig. 2d). Next we segmented the prostate on I_{US} using an automatic segmentation method which is a 3D extension of our previous work (Zeng et al., 2018). The prostate surface extracted from the annotated MRI, I_{MR}, is non-rigidly registered to the surface computed by the automatic segmentation of the 3D TRUS volume, I_{US}, using the coherent point drift method by Myronenko and Song (2010). The registered prostate surface is overlaid onto I_{US} and displayed on our user interface. In case of inconsistencies, this boundary could be manually modified by the clinician to match the visible prostate outline (see Fig. 5). The clinician can apply a set of rigid (translation and rotation), affine (shrinking and expanding along three axes) and non-rigid transformations. The latter step is applied by dragging and dropping points on the prostate. After each surface registration step (automatic and manual), the displacement between the initial and final positions of a modified point $d = P_i - P_f$ is computed and applied to the mesh nodes of its enclosing element. The K matrix is updated based on the new boundary condition and the displacement of the rest of the nodes is computed $u_r = K' u_s$. This step takes $\approx 0.1s$ (Fig. 2e). We can now compute a transformation $T_{\text{MR-TRUS}}$ to deform the mesh elements and their enclosing voxels from the MR image into the TRUS coordinate frame. However, to keep the method real-time we avoid the computationally expensive task of deforming the entire MR volume based on the updated FEM mesh. Instead, we employ a real-time algorithm that can render any arbitrary 2D slice in a deformed volume (Goksel and Salcudean, 2009). This will be explained in more details in the next section. If deemed necessary by the surgeon because of prostate motion, the TRUS volume acquisition and registration may be repeated during the surgery in order to update the registration.

3.3. Real-time deformed MRI rendering

To display the deformed MRI and project it on the prostate mesh, we employ a finite element-based algorithm for fast synthesis of 2D slices in a deformed 3D volume presented in (Goksel and Salcudean, 2009). For each pixel p in the 2D slice, the following steps are taken:

(I) Find the finite element e_s enclosing p
(II) Find the undeformed location of p^0 based on the nodal displacements of e_s
(III) Interpolate the MRI volume at p^0.

We used the efficient scheme proposed by Goksel and Salcudean (2009) to assign each pixel to a mesh element in constant time. In involves compiling the set of all elements $\{e_s\}$ that are intersected by the 2D TRUS imaging plane, topologically sorting them, marking their cross-section on the image pixels and finally traversing the image and the marked cross-sections with parallel scan lines.

3.4. Image guidance interface

Fig. 3 displays a snap-shot of the image guidance interface during a RALRP procedure. It consists of two sub-windows: The one on the left displays the reconstructed 3D surgery scene (Fig. 3.a) and the one on the right displays the live TRUS B-Mode images (Fig. 3.b).

The 3D scene consists of: (i) a 2D axial slice of the MR volume at the axial position of the da Vinci instrument tip and projected on the prostate mesh, (ii) a 3D surface mesh of the prostate built from the segmentation of the preoperative MRI and deformed based on the registration to the intraoperative 3D TRUS image; this mesh is clipped against the MRI axial plane to remove the mesh elements that would obstruct the view of the MRI (see Fig. 6), (iii) A 2D plane placed at the same position and orientation as the actual TRUS plane to help the surgeon locate the TRUS image relative to the other elements (see Fig. 6d), (iv) 3D models of the TRUS probe and the da Vinci surgical instrument (Fig. 6d), and (v) a virtual endoscope through which the scene is viewed. All of the virtual elements (prostate, TRUS probe, surgical instrument and the endoscope) are registered to the da Vinci coordinate system and have

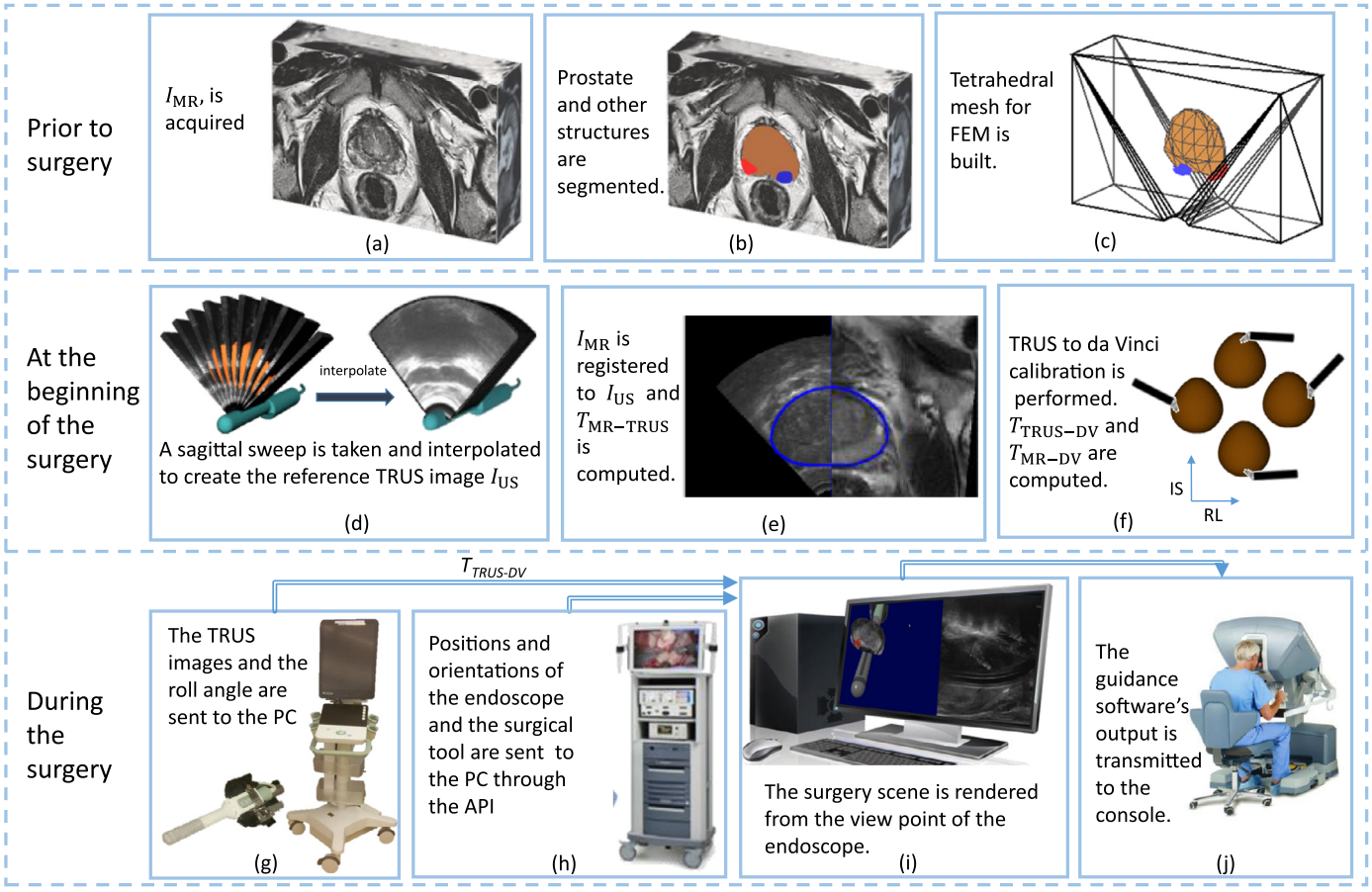

Fig. 2. Prior to the surgery (a) A T_2-weighted magnetic resonance image, I_{MR} is acquired, (b) the prostate and the structures of interest such as tumors are segmented by a radiologist, based on which (c) a tetrahedral mesh M and a finite element model are built. On the intervention day (d) a 3D TRUS image I_{US} is acquired by rotating the TRUS sagittal imaging plane fully through the prostate and interpolating the resulting sagittal images. (e) I_{MR} is then deformably registered to I_{US} by updating the prostate mesh M. (f) TRUS to da Vinci registration is performed ($T_{TRUS\text{-}DV}$ and $T_{MR\text{-}DV}$ are computed). During the surgery, (g) live 2D TRUS images are acquired, (h) the positions and orientations of the endoscope and the surgical tool are sent to the PC through the API, (i) The surgery scene is rendered from the view point of the endoscope. The 3D prostate mesh is clipped at the instrument tip and the axial slice in the registered I_{MR} is projected on it. (j) The guidance software output is transmitted to the console to be displayed using da Vinci's TilePro™ system.

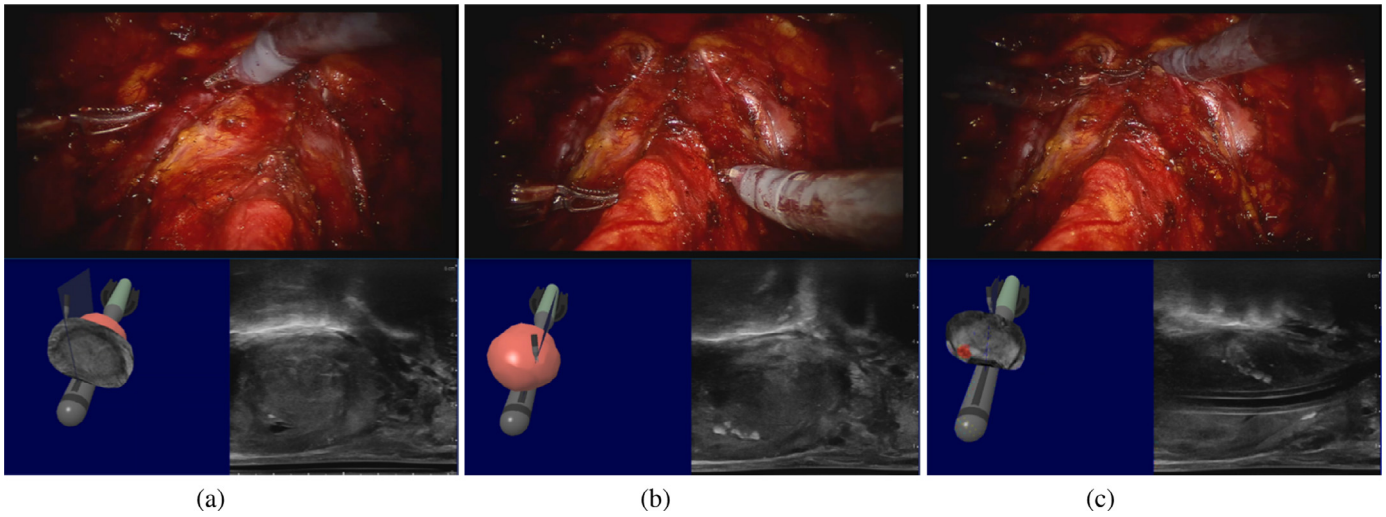

Fig. 3. (a–c) The surgeon's view during one of our patient studies is displayed at three different time points. On top is the endoscope's output, below right is the live B-Mode image and below left is the 3D surgery scene. The TRUS imaging plane is rendered in solid dark blue in the 3D scene to help the surgeon visualize at which position and orientation the US plane lies relative to the prostate. The delineated tumour is identified by a red overlay. (For interpretation of the references to color in this figure legend, the reader is referred to the web version of this article.)

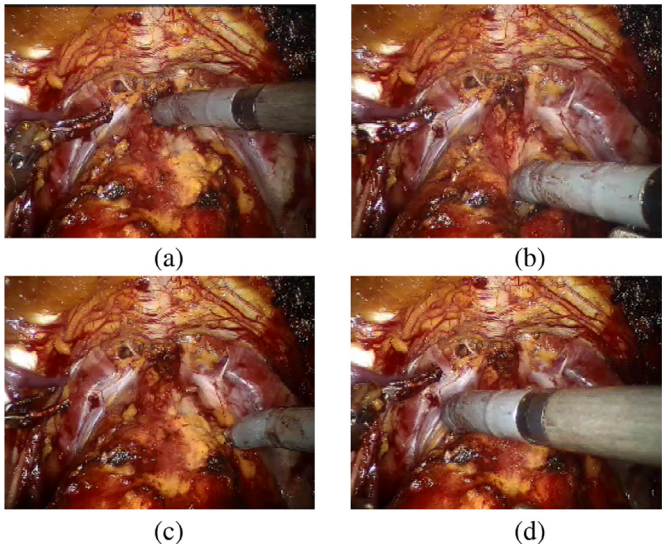

Fig. 4. The calibration of the robotic TRUS involves finding a transformation from the TRUS coordinate system to the da Vinci coordinate system. To this end, the tip of the da Vinci instrument is identified at a minimum of four locations on the tissue surface in the TRUS image. These points included (a) a point on the apex and the midline, (b) a point on the base and the midline, (c) a point on the patient's right and migland (d) and a point on the patient's left and midgland.

the same position and orientation as their real-world counterparts. Hence, the virtual scene is a 3D reconstruction of the surgeon's surgical view. Whereas the orientation and position of the virtual camera is determined by the real endoscope, the zoom level is determined by the surgeon and can be changed in real-time during the surgery. Zooming in allows for better viewing of the details on the MRI, while zooming out provides an overview of the entire surgery scene. Additionally, live B-Mode images are captured from the ultrasound machine and transmitted to the external PC and displayed next to the surgery scene. The output of our guidance software is rendered separately for the left and the right eye and the outputs are connected to the specific ports on the TilePro^{TM} multi-input display of the da Vinci console to give the surgeon a true 3D experience.

3.5. Computation time and transmission latency

Our software has two primary sources of input: (I) The da Vinci Research API stream is fed to the desktop through a standard ethernet cable using a TCP/IP connection. (II) The BlackMagic Decklink Quad 2 frame grabber card captures frames from the BK3500 ultrasound machine at a resolution of 1920×1080. This signal is in the HDMI format and is converted to SDI using a BlackMagic mini converter.

Our software's output to the da Vinci TilePro console is a stereo 3D signal sent using the DeckLink Quad 2 card through SDI cables and is handled through a separate thread by the Decklink Quad API.

To evaluate the latency of the Decklink Quad 2 system, a stopwatch was started on a test computer. This display signal was then captured by the DeckLink Quad 2 card and sent to the da Vinci Console. A camera was then used to capture all the displays in order to obtain the time-stamp on each screen. The results can be seen in Table 2 (computation time deviations from the reported numbers are negligible). To compute the total latency of this multi-threaded system, we added the latency of each separate thread. Since the ultrasound input is not involved in the main processing loop, its latency does not need to be added to the scene rendering computation time. The US signal has a total latency of 200.0 ms.

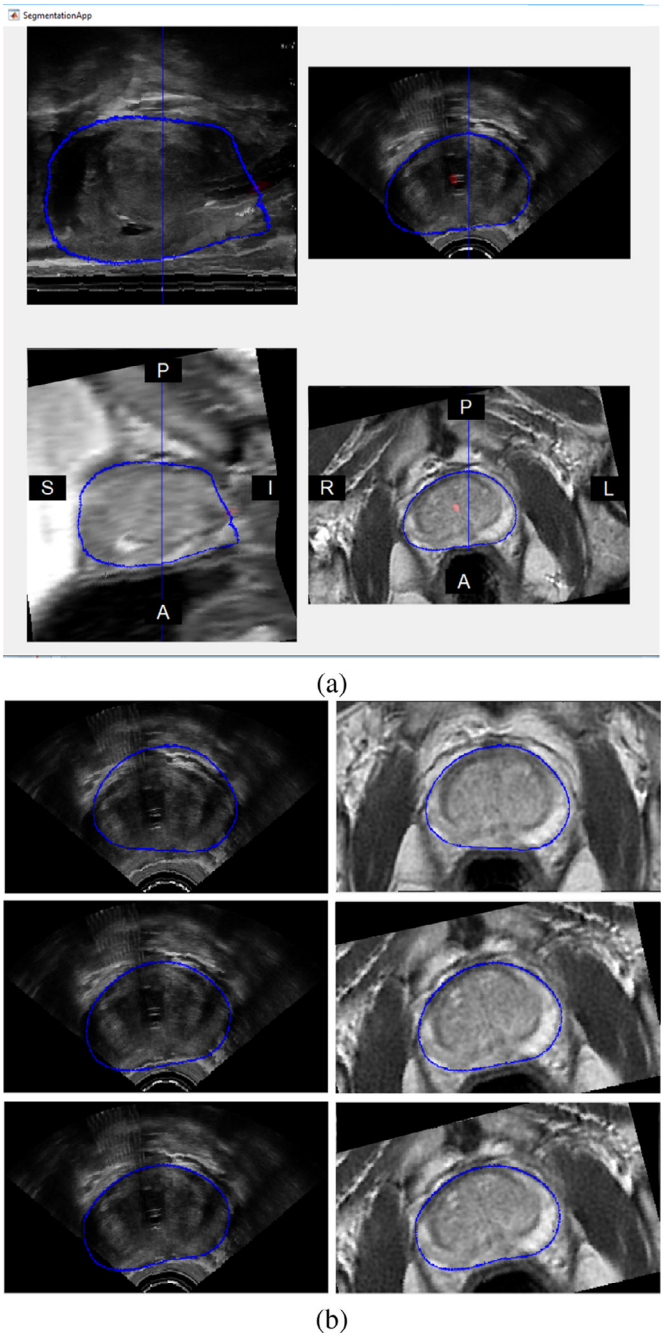

Fig. 5. (a) View of our interactive registration application. The prostate surface boundary extracted from the annotated MRI is overlaid on I_{US}. This boundary is first automatically and then if needed manually manipulated by the clinician to match the visible prostate outline. (b) The registration results for a typical MR-TRUS pair are displayed for an axial slice near midgland. The top row is the initial alignment, the middle row is the registration results after the rigid alignment and the bottom row is the result of the final non-rigid registration.

The total latency time for the rendered scene in the da Vinci console was 144.4 ms and consisted of the latency of the da Vinci API, the scene rendering time, deformed MRI rendering and the TilePro output.

4. Phantom studies

The purpose of the phantom experiments were to measure the combined error of the MR-TRUS registration and TRUS-da Vinci calibration processes. To that end, the proposed system was tested us-

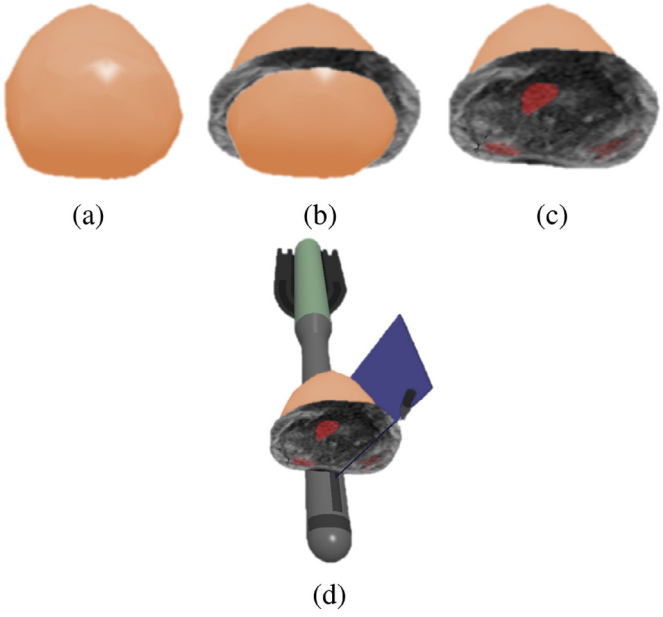

Fig. 6. This figure demonstrates the steps for rendering the virtual surgery scene. (a) The surface mesh of the prostate is built from the segmentation on the preoperative MRI and deformed after registration to the intraoperative 3D TRUS. (b) The MRI volume is re-sliced with an axial plane at the position of the instrument tip and displayed inside the mesh at its correct position. (c) The mesh is clipped axially at the tool tip to remove the mesh elements that would obstruct the view to the MRI. (d) A 2D plane (in blue) is displayed at the same position and orientation as the actual TRUS plane to help the surgeon locate the TRUS image relative to the other elements. The TRUS transducer and the instrument are also rendered at their correct positions relative to the prostate. (For interpretation of the references to color in this figure legend, the reader is referred to the web version of this article.)

Table 2
Transmission latency and computation time for signals and connections in our system. All of these signals have a frequency of 60 Hz.

Signal / connection	Computation time / latency
Da Vinci API	2.0 ± 1.67 ms
3D scene rendering	15.1 ± 2.0 ms
Deformed MRI rendering	2.6 ± 0.29 ms
Ultrasound to desktop (through Decklink Quad 2)	75.0 ± 14.8 ms
Desktop to da Vinci TilePro™	125 ± 17.6 ms
Total latency of rendered scene	144.4 ms
Total latency of displayed US	200.0 ms

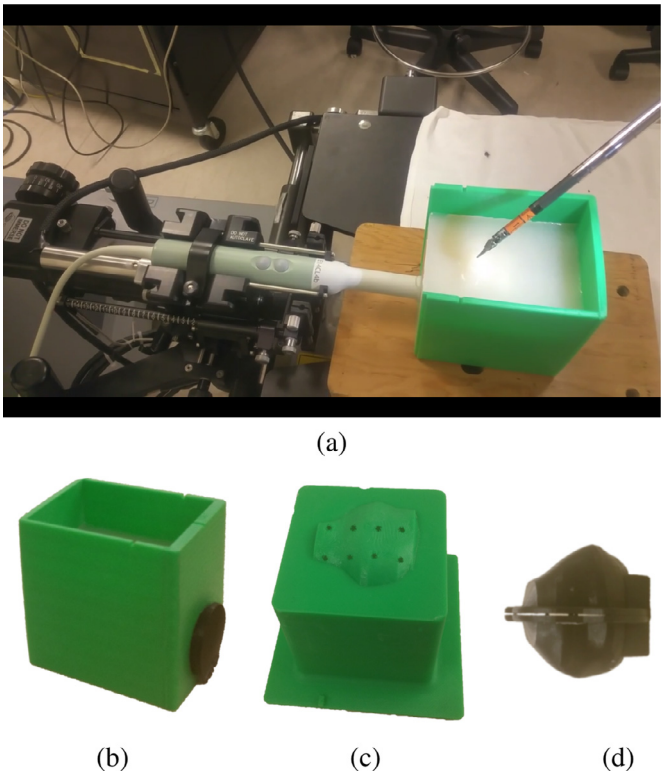

Fig. 7. (a) The fabricated phantom being used during an experiment. (b-d) The 3D-printed molds for our phantom studies are displayed. Item (b) is the container that holds the entire phantom and has a fitted black shaft to create a cylindrical canal for the probe placement. Item (c) is the negative prostate mold that is placed inside the container to create the posterior imprint of the prostate and the beads on the surface. Item (d) is the prostate mold that is built based on the patient's prostate segmented on a T2 MRI.

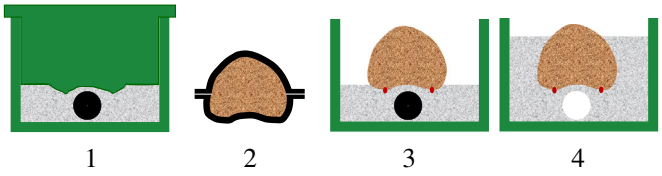

Fig. 8. Step 1: A container (item b in Fig. 7) is half filled with agar mixture and a negative mold (item c in Fig. 7) is placed and allowed to settle. Step 2: The prostate phantom is built separately using a 3D printed mold (item d in Fig. 7). Step 3: The beads are placed at the dents imprinted on the prostate phantom and the prostate phantom is placed in the tissue phantom depression. Step 4: The first agar mixture is added again to completely cover the prostate phantom. When it is set, the black shaft is removed to create the canal for inserting the TRUS probe.

ing a custom-made prostate phantom with two regions, one for the prostate and one for the bulk tissue surrounding the organ (Fig. 7). To mimic the surgery conditions, we built our phantom based on a patient's anatomy using 3D printed molds. The components consist of: (i) an outer container for holding the entire phantom, *i.e.*, the prostate and the surrounding tissue with a shaft that is placed inside the container to create a cylindrical canal mimicking the rectum where the probe will be placed (Fig. 7.b), (ii) a negative mold for creating the prostate depression on the lower part which has the imprint of the anterior of the prostate on its surface to allow for seamless placement of the prostate phantom on its top (Fig. 7c), and (iii) eight small plastic beads to be used as fiducials as they can be easily localized in the ultrasound image. They lie on two rows (each containing four beads) posterior to the prostate phantom (see Fig. 7c), which is cast in a 3D-printed prostate mold obtained from the segmented prostate of the patient in the MRI (Fig. 7d).

Fig. 8 illustrates the different steps of our phantom fabrication process. First the outer container is half filled with the agar mixture, where the negative mold is placed and allowed to settle. The prostate phantom is built separately with a denser agar mixture to make the two regions distinguishable. Then, the beads are placed at the dents imprinted on the prostate phantom. Finally the prostate phantom is placed in the tissue phantom depression and the first agar mixture is added again to completely cover the prostate phantom.

4.1. Experiments

To conduct the experiments, the TRUS transducer is placed inside the rectal canal of the phantom. The TRUS to da Vinci calibration is performed as in surgery, as described in Section 3.1. Next, a TRUS sweep is carried out and a 3D image is obtained (See Fig. 9). The positions of the beads on the TRUS image are manually

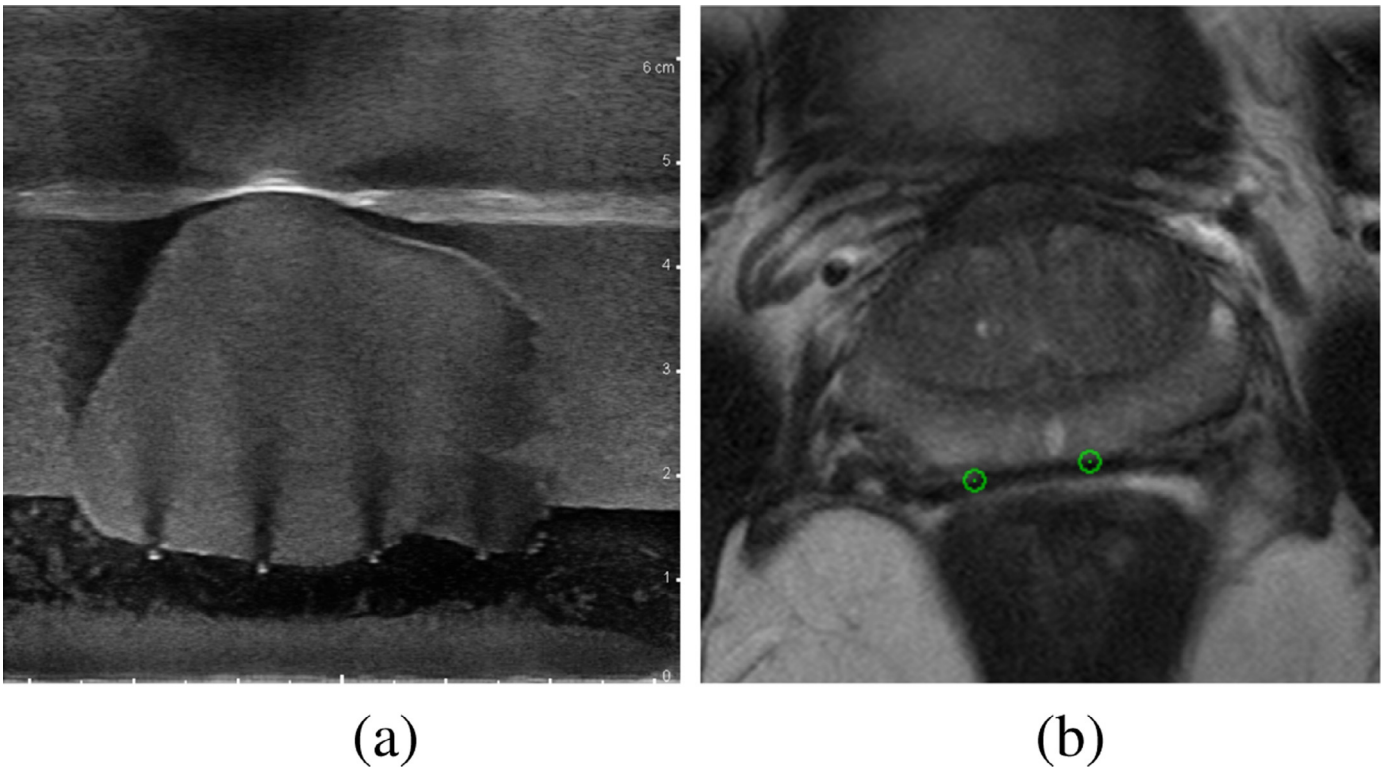

Fig. 9. (a) A sagittal TRUS image of the phantom close to the midline. The four beads in a row can be seen. (b) An axial slice of the MRI with the position of the beads in the 3D mesh marked as green circles. (For interpretation of the references to color in this figure legend, the reader is referred to the web version of this article.)

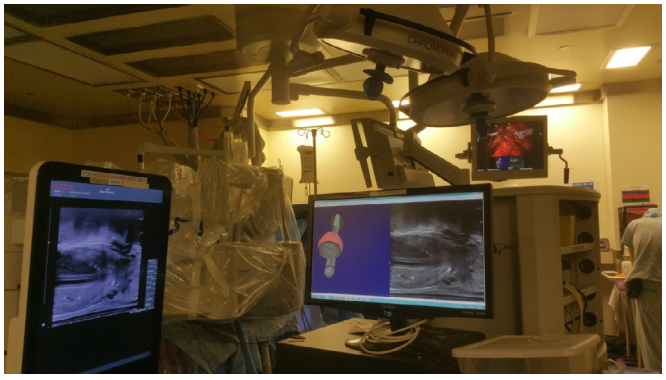

Fig. 10. Our hardware setup in the operating room. The TRUS probe is mounted on the stepper and placed before the surgery starts. Next, the da Vinci robot is docked. The US machine is connected to the PC and the images are transferred to the guidance software. The MR-TRUS registration is completed and the virtual surgery scene is rendered. The virtual surgery scene and the B-mode image are transferred to the surgeon's console and displayed under the endoscope's feed (as can be seen on the endoscopic video display on the top right of the image).

found. The TRUS image is registered to the pre-op MRI with the annotated beads as described in Section 3.2. The deformed MRI is displayed on the da Vinci console. The phantom is removed and replaced with a container filled with water without moving the probe, hence preserving the TRUS-da Vinci calibration. The operator is asked to sit at the console and place the displayed virtual da Vinci instrument on one of the marked beads. A sweep is taken, the instrument tip is manually located in the TRUS image and its position is recorded. This is repeated for all 8 beads. The actual position of the beads in the TRUS volume is compared with the instrument position and the difference is reported as the error. We repeated this experiment with 4 subjects. The average error of 8 beads for these subjects are presented in Table 3.

Table 3
Phantom study results.

Subject	Error
1	3.1 ± 1.2
2	3.0 ± 1.5
3	2.8 ± 1.2
4	3.9 ± 1.2
mean	3.19 ± 1.30

5. *In vivo* patient studies

The clinical procedure is similar to our previous study (Mohareri et al., 2015b). The main components of the system during this clinical study inside the operating room are shown in Fig. 1. The patients underwent preoperative mp-MRI and a radiologist was asked to examine their MRI volume and contour the prostate and the lesions. The lesions were identified and reported according to PI-RADS V2 (Weinreb et al., 2016).

Before the start of the surgery, the TRUS probe was placed using the brachytherapy stabilizer arm. Initial steps of the surgery are performed as usual using a suitable approach. After the endopelvic fascia were exposed, the TRUS coordinate system was registered to the da Vinci coordinate system (as described in Section 3.1). Next, a 3D TRUS volume was taken and the annotated T2 MRI was registered to it according to the method described in Section 3.2. Live B-mode images, the registered MRI and the 3D surgical scene were rendered and displayed on the surgeon's console as described in Section 3.4.

5.1. Results

To date, 12 patients with clinically organ confined prostate cancer undergoing RALRP have participated in our institutional review board approved study. We were able to successfully employ our

system in the operating room for these patients. Our system ran continuously during the surgeries, did not interfere with their normal course and was used several times per surgery to orient the surgeon with respect to the anatomy. The surgeon had positive feedback on our system and routinely used it during bladder neck dissection and to discuss the surgery plan with surgical trainees. By viewing the surface of the 3D prostate model and moving the surgical instrument from base to apex, the surgeon could confirm that the MRI and the 3D virtual prostate align well with the observed organ through the endoscope. Furthermore, the availability of the annotated MRI at the surgeon's console and the ease of navigating through the slices and viewing the location of the tumour inside the organ relative to his surgical instrument were deemed useful during the surgery. The TRUS acquisition took 30 seconds and the registration of pre-op MR to it took on average 2 minutes. This process was performed any time the surgeon wished to use our system. To evaluate the accuracy of our TRUS-da Vinci calibration, we recorded an additional set of corresponding TRUS-da Vinci instrument tip positions in the last 8 cases. We used the calculated TRUS-da Vinci transformation and the instrument tip position in the TRUS coordinate system to compute the da Vinci coordinates and compared this to the actual da Vinci read-out. The average error for these 8 cases was 1.4 $\pm$ 0.3 mm. We also identified 24 landmarks on the registered MR and the corresponding TRUS images of these 8 cases (3 landmarks per patient). The average target registration error for these 24 landmarks was 2.1 $\pm$ 0.8 mm. Given the TRUS-da Vinci calibration error of 1.4 mm and the TRUS-MRI registration error of 2.1 mm, we expect the overall average error (da Vinci-MRI registration) to be smaller than 3.5 mm. This is close to the mean error in our phantom studies (3.2 $\pm$ 1.3 mm).

6. Discussion

At this stage of our study, the output of our software is displayed underneath the endoscope's feed and not overlaid on it. To be able to correctly augment the endoscopic video as the camera moves by using the robot kinematics, it is necessary to acquire more accurate measurements of the endoscope parameters. These include intrinsic (focal length, pixel aspect ratio, etc.) and extrinsic parameters (the exact camera position and orientation). To obtain the former, an accurate camera calibration has to be performed anytime the surgeon changes the focus of the camera. As for the latter, the position and orientation received through the API do not correspond to the endoscope but to the robotic end-effector where the camera is mounted. To find the precise extrinsic parameters for the endoscope, a so-called *hand-eye* transformation between the endoscopic camera and the robot coordinate system has to be computed. These issues have been addressed to a large extent in the most recent da Vinci model (Xi) by using a focus-free endoscope, which greatly simplifies the hand-eye calibration. In the future, we expect to be able to transition to an augmented reality system that overlays the image on top of the endoscope view, with the use of newly developed camera and hand-eye calibration approaches, or with the use of an Xi system.

The algorithms and methods used in our system have been designed to accommodate for the intraoperative changes to the prostate mesh model. These include rendering of an MR slice in real-time without the need to deform the entire MR volume in the presence of prostate deformations (see Section 3.3). While the TRUS acquisition and MR-TRUS registration could be performed at any point during the surgery, the added 2 min to the surgery time made the surgeon hesitant to use it frequently. Future work will incorporate our real-time, non-rigid registration of 3D MRI to 2D B-mode TRUS for continuous registration and update to the prostate shape and MRI (Samei et al., 2018). This will provide more reliable guidance throughout the surgery in the presence of prostate motion and deformation.

7. Conclusion

In this work, we have described a novel image guidance system for RALRP. To the best of our knowledge, it is the first instance of a clinically deployed MRI-TRUS guidance system for prostatectomy where the preoperative MRI is non-rigidly registered to live TRUS images. Our system displays the deformed MRI at the surgeon's console and the non-rigid registration could be computed at multiple times during the surgery with minimal need for operator intervention. Moreover, the surgeon can use a da Vinci instrument to rotate the transducer and determine the imaging planes of the live TRUS as well the registered MRI volume. This is an intuitive and convenient way for the surgeon to explore both of the provided imaging modalities from their console. Furthermore, by incorporating our method of real-time, non-rigid 3D to 2.5 D TRUS registration (Samei et al., 2018), our system has the potential to deform the MRI volume in real-time. Finally, since the scene is rendered from the viewpoint of the endoscope, given correct parameters of the camera, an augmented scene can be overlaid on the video output. We believe that our system has the potential to improve the outcomes of RP by providing the surgeon with real-time image-guidance that accurately shows the prostate anatomy and the prostate cancer location and its proximity to critical structures. The results of this work motivate further studies to quantitatively assess the influence of our system on functional and oncological success.

Declaration of Competing Interest

I wish to confirm that there are no known conflicts of interest associated with this publication and there has been no significant financial support for this work that could have influenced its outcome.

Acknowledgments

We are thankful for financial support provided by the Canadian Institutes of Health Research (CIHR MOP-142439) and the Charles Laszlo Chair in Biomedical Engineering held by Professor Septimiu Salcudean.

References

Adebar, T., Salcudean, S., Mahdavi, S., Moradi, M., Nguan, C., Goldenberg, L., 2011. A robotic system for intra-operative trans-rectal ultrasound and ultrasound elastography in radical prostatectomy. In: International Conference on Information Processing in Computer-Assisted Interventions. Springer, pp. 79–89.

Bernhardt, S., Nicolau, S.A., Soler, L., Doignon, C., 2017. The status of augmented reality in laparoscopic surgery as of 2016. Med. Image Anal. 37, 66–90.

Cepek, J., Chronik, B.A., Lindner, U., Trachtenberg, J., Davidson, S.R.H., Bax, J., Fenster, A., 2013. A system for MRI-guided transperineal delivery of needles to the prostate for focal therapy. Med. Phys. 40 (1), 012304.

Cohen, D., Mayer, E., Chen, D., Anstee, A., Vale, J., Yang, G.-Z., Darzi, A., et al., 2010. Augmented reality image guidance in minimally invasive prostatectomy. In: International Workshop on Prostate Cancer Imaging. Springer, pp. 101–110.

DiMaio, S., Hasser, C., 2008. The da Vinci research interface. MIDAS J. Syst. Archit. Comput. Assist. Interv.. Available at http://hdl.handle.net/10380/1464.

Ficarra, V., Novara, G., Artibani, W., Cestari, A., Galfano, A., Graefen, M., Guazzoni, G., Guillonneau, B., Menon, M., Montorsi, F., et al., 2009. Retropubic, laparoscopic, and robot-assisted radical prostatectomy: a systematic review and cumulative analysis of comparative studies. Eur. Urol. 55 (5), 1037–1063.

Fischler, M.A., Bolles, R.C., 1981. Random sample consensus: a paradigm for model fitting with applications to image analysis and automated cartography. Commun. ACM 24 (6), 381–395.

Goksel, O., Salcudean, S.E., 2009. B-Mode ultrasound image simulation in deformable 3-D medium. Med. Imaging IEEE Trans. 28 (11), 1657–1669.

Haglind, E., Carlsson, S., Stranne, J., Wallerstedt, A., Wilderäng, U., Thorsteinsdottir, T., Lagerkvist, M., Damber, J.-E., Bjartell, A., Hugosson, J., et al., 2015. Urinary incontinence and erectile dysfunction after robotic versus open radical

prostatectomy: a prospective, controlled, nonrandomised trial. Eur. Urol. 68 (2), 216–225.
Han, M., Kim, C., Mozer, P., Schäfer, F., Badaan, S., Vigaru, B., Tseng, K., Petrisor, D., Trock, B., Stoianovici, D., 2011. Tandem-robot assisted laparoscopic radical prostatectomy to improve the neurovascular bundle visualization: a feasibility study. Urology 77 (2), 502–506.
Hung, A.J., De Castro, A.A.L., Shoji, S., Goh, A.C., Berger, A.K., Desai, M.M., Aron, M., Gill, I.S., Ukimura, O., 2012. Robotic transrectal ultrasonography during robot-assisted radical prostatectomy. Eur. Urol. 62 (2), 341–348.
Kolagunda, A., Sorensen, S., Mehralivand, S., Saponaro, P., Treible, W., Turkbey, B., Pinto, P., Choyke, P., Kambhamettu, C., 2018. A mixed reality guidance system for robot assisted laparoscopic radical prostatectomy. In: OR 2.0 Context-Aware Operating Theaters, Computer Assisted Robotic Endoscopy, Clinical Image-Based Procedures, and Skin Image Analysis. Springer, pp. 164–174.
Kratiras, Z., Gavazzi, A., Belba, A., Willis, B., Chew, S., Allen, C., Amoroso, P., Dasgupta, P., 2018. Phase I study of a new tablet based image guided surgical system in robotic assisted radical prostatectomy. Minerva Urol. Nefrol. 71 (1), 92–95.
Logan, J.K., Rais-Bahrami, S., Turkbey, B., et al., 2013. Current status of MRI and ultrasound fusion software platforms for guidance of prostate biopsies [published online ahead of print december 3, 2013]. BJU Int. 114 (5), 641–652.
Long, J.-A., Lee, B.H., Guillotreau, J., Autorino, R., Laydner, H., Yakoubi, R., Rizkala, E., Stein, R.J., Kaouk, J.H., Haber, G.-P., 2012. Real-time robotic transrectal ultrasound navigation during robotic radical prostatectomy: initial clinical experience. Urology 80 (3), 608–613.
Marks, L., Young, S., Natarajan, S., 2013. Mri–ultrasound fusion for guidance of targeted prostate biopsy. Curr. Opin. Urol. 23 (1), 43.
Martini, A., Wagaskar, V.G., DellOglio, P., Rastinehad, A.R., Sfakianos, J.P., Tewari, A.K., 2019. Image guidance in robot-assisted radical prostatectomy: how far do we stand? Curr. Opin. Urol. 29 (1), 10–13.
McClure, T.D., Margolis, D.J.A., Reiter, R.E., Sayre, J.W., Thomas, M.A., Nagarajan, R., Gulati, M., Raman, S.S., 2012. Use of MR imaging to determine preservation of the neurovascular bundles at robotic-assisted laparoscopic prostatectomy. Radiology 262 (3), 874–883.
Mohareri, O., Ischia, J., Black, P.C., Schneider, C., Lobo, J., Goldenberg, L., Salcudean, S.E., 2015. Intraoperative registered transrectal ultrasound guidance for robot-assisted laparoscopic radical prostatectomy. J. Urol. 193 (1), 302–312.
Mohareri, O., Nir, G., Lobo, J., Savdie, R., Black, P., Salcudean, S., 2015. A system for MR-ultrasound guidance during robot-assisted laparoscopic radical prostatectomy. In: International Conference on Medical Image Computing and Computer-Assisted Intervention. Springer, pp. 497–504.
Moore, C.M., Robertson, N.L., Arsanious, N., Middleton, T., Villers, A., Klotz, L., Taneja, S.S., Emberton, M., 2013. Image-guided prostate biopsy using magnetic resonance imaging–derived targets: a systematic review. Eur. Urol. 63 (1), 125–140.
Myronenko, A., Song, X., 2010. Point set registration: coherent point drift. IEEE Trans. Pattern Anal. Mach. Intell. 32 (12), 2262–2275.
Nir, G., Sahebjavaher, R.S., Kozlowski, P., Chang, S.D., Sinkus, R., Goldenberg, S.L., Salcudean, S.E., 2013. Model-based registration of ex vivo and in vivo MRI of the prostate using elastography. IEEE Trans. Med. Imaging 32 (6), 1068–1080.
Pinto, P.A., Chung, P.H., Rastinehad, A.R., Baccala Jr, A.A., Kruecker, J., Benjamin, C.J., Xu, S., Yan, P., Kadoury, S., Chua, C., et al., 2011. Magnetic resonance imaging/ultrasound fusion guided prostate biopsy improves cancer detection following transrectal ultrasound biopsy and correlates with multiparametric magnetic resonance imaging. J. Urol. 186 (4), 1281–1285.
Porpiglia, F., Bertolo, R., Amparore, D., Checcucci, E., Artibani, W., Dasgupta, P., Montorsi, F., Tewari, A., Fiori, C., 2018. Augmented reality during robot-assisted radical prostatectomy: expert robotic surgeons' on-the-spot insights after live surgery. Minerva Urol. Nefrol. 70 (2), 226–229.
Porpiglia, F., Bertolo, R., Checcucci, E., Amparore, D., Fiori, C., 2018. 3D augmented reality robot-assisted radical prostatectomy. Eur. Urol. Suppl. 17 (2), e1929.
Porpiglia, F., Checcucci, E., Amparore, D., Autorino, R., Piana, A., Bellin, A., Piazzolla, P., Massa, F., Bollito, E., Gned, D., et al., 2018. Augmented-reality robot-assisted radical prostatectomy using hyper-accuracy three-dimensional reconstruction (HA 3D) technology: a radiological and pathological study. BJU Int. 17 (7), e2287.
Porpiglia, F., Fiori, C., Checcucci, E., Amparore, D., Bertolo, R., 2018. Augmented reality robot-assisted radical prostatectomy: preliminary experience. Urology 115, 184.
Samei, G., Goksel, O., Lobo, J., Mohareri, O., Black, P., Rohling, R., Salcudean, S., 2018. Real-time FEM-based registration of 3D to 2.5D transrectal ultrasound images. IEEE Trans. Med. Imaging 37 (8), 1877–1886.
Simpfendörfer, T., Baumhauer, M., Müller, M., Gutt, C.N., Meinzer, H.-P., Rassweiler, J.J., Guven, S., Teber, D., 2011. Augmented reality visualization during laparoscopic radical prostatectomy. J. Endourol. 25 (12), 1841–1845.
Sridhar, A.N., Hughes-Hallett, A., Mayer, E.K., Pratt, P.J., Edwards, P.J., Yang, G.-Z., Darzi, A.W., Vale, J.A., 2013. Image-guided robotic interventions for prostate cancer. Nat. Rev. Urol. 10 (8), 452.
Susil, R.C., Camphausen, K., Choyke, P., McVeigh, E.R., Gustafson, G.S., Ning, H., Miller, R.W., Atalar, E., Coleman, C.N., Ménard, C., 2004. System for prostate brachytherapy and biopsy in a standard 1.5 T MRI scanner. Magn. Reson. Med. 52 (3), 683–687.
Tan, N., Margolis, D.J.A., McClure, T.D., Thomas, A., Finley, D.S., Reiter, R.E., Huang, J., Raman, S.S., 2012. Radical prostatectomy: value of prostate MRI in surgical planning. Abdom. Imaging 37 (4), 664–674.
Thompson, S., Penney, G., Billia, M., Challacombe, B., Hawkes, D., Dasgupta, P., 2013. Design and evaluation of an image-guidance system for robot-assisted radical prostatectomy. BJU int. 111 (7), 1081–1090.
Ukimura, O., Aron, M., Nakamoto, M., Shoji, S., de Castro, A.A.L., Matsugasumi, T., Berger, A., Desai, M., Gill, I.S., 2014. Three-dimensional surgical navigation model with TilePro display during robot-assisted radical prostatectomy. J. Endourol. 28 (6), 625–630.
Ukimura, O., Gill, I.S., 2008. Imaging-assisted endoscopic surgery: cleveland clinic experience. J. Endourol. 22 (4), 803–810.
Ukimura, O., Magi-Galluzzi, C., Gill, I.S., 2006. Real-time transrectal ultrasound guidance during laparoscopic radical prostatectomy: impact on surgical margins. J. Urol. 175 (4), 1304–1310.
Villeirs, G.M., De Meerleer, G.O., 2007. Magnetic resonance imaging (MRI)| anatomy of the prostate and application of MRI in radiotherapy planning. Eur. J. Radiol. 63 (3), 361–368.
Weinreb, J.C., Barentsz, J.O., Choyke, P.L., Cornud, F., Haider, M.A., Macura, K.J., Margolis, D., Schnall, M.D., Shtern, F., Tempany, C.M., et al., 2016. Pi-rads prostate imaging–reporting and data system: 2015, version 2. Eur. Urol. 69 (1), 16–40.
Zeng, Q., Samei, G., Karimi, D., Kesch, C., Mahdavi, S.S., Abolmaesumi, P., Salcudean, S.E., 2018. Prostate segmentation in transrectal ultrasound using magnetic resonance imaging priors. Int. J. Comput. Assist. Radiol. Surg. 13 (6), 749–757.